



Soft, wireless electronic dressing system for wound analysis and biophysical therapy



Seung Min Yang^{a,1}, Hyerim Kim^{b,1}, Gwan-Jin Ko^{a,1}, Jong Chan Choe^a, Joong Hoon Lee^a, Kaveti Rajaram^a, Byoungha An^{c,d}, Won Bae Han^a, Dong-Je Kim^a, Jeong-Woong Shin^a, Tae-Min Jang^a, Heeseok Kang^a, Sungkeun Han^a, Kangwon Lee^{e,f}, Seung Ja Oh^{g,*}, Suk-Won Hwang^{a,c,h,**}

^a KU-KIST Graduate School of Converging Science and Technology, Korea University, Seoul 02841, Republic of Korea

^b Program in Nanoscience and Technology, Graduate School of Convergence Science and Technology, Seoul National University, Seoul 08826, Republic of Korea

^c Center for Biomaterials, Biomedical Research Institute, Korea Institute of Science and Technology (KIST), Seoul 02792, Republic of Korea

^d Division of Bio-Medical Science & Technology, KIST School, University of Science and Technology (UST), Seoul 02792, Republic of Korea

^e Department of Applied Bioengineering, Graduate School of Convergence Science and Technology, Seoul National University, Seoul 08826, Republic of Korea

^f Research Institute for Convergence Science, Seoul National University, Seoul 08826, Republic of Korea

^g Department of Genetics and Biotechnology, College of Life Sciences, Kyung Hee University, Yongin-si 17104 Gyeonggi-do, Republic of Korea

^h Department of Integrative Energy Engineering, Korea University, Seoul 02841, Republic of Korea

ARTICLE INFO

Article history:

Received 31 July 2022

Received in revised form 26 September 2022

Accepted 6 November 2022

Available online xxxx

Keywords:

Smart wound dressing

Wireless wearable platform

Inflammation sensor

Electrical stimulation

Wound healing

ABSTRACT

Advances in wearable technology promise effective strategies to improve the management of patients, particularly systematic wound monitoring tools combined with wireless therapeutic stimulation provide medical and allied health professions with unprecedented insight for inpatients/outpatients beyond traditional nursing environments. Here, we introduce a soft, wireless electronic wound dressing system that can offer both real-time monitoring of wound status, and biophysical therapy for acceleration of wound repairing rates, in a completely integrated form. Synthetic hydrogel-based sensor responds to a biochemical marker (i.e., cathepsin) released from the inflammatory reaction, while electronic sensor arrays collect humidity, pH, and temperature related to the healing process. Miniaturized circuit components serve wireless measurements via Bluetooth interfaces and provide programmed patterns of electrical/optical stimulations that can promote the recovery of damaged tissues. *In vivo* demonstrations illustrate capabilities of systematic medical care in freely behaving mice, thereby suggesting potential for use in advanced medic-free wound managements.

© 2022 Elsevier Ltd. All rights reserved.

Introduction

Wearable, implantable electronic systems formed by soft, flexible materials or structures provide a variety of favorable functions, ranging from monitors of physical fitness and activity, and physiological signals to the prevention, treatment and management of illness as forms of smartwatch, eyewear, electronic skin (e-skin) and

biomedical implants [1–11]. Relevant technologies include ultrathin and miniaturized sensors, AR/VR platforms, optogenetics, drug delivery systems, and electrical/optical stimulation, all of which have been evolved toward high precision of diagnosis, therapy and prognosis as well as user- or patient-specific directions as a personalized healthcare [8,12–21]. In this context, such research efforts have delivered innovative approaches to manage and treat types of skin wounds, particularly for elderly and chronic patients requiring long-term or effective care. Exemplified demonstrations provided ways to detect key physical, biochemical parameters such as pH, temperature, uric acid, nitrogen oxide and bacterial growth, which contains valuable information for quantitative assessments of wound status [22–26]. As for treatment, electrical and optical stimulation in various modes has been suggested to promote the repair

* Corresponding author.

** Corresponding author at: KU-KIST Graduate School of Converging Science and Technology, Korea University, Seoul 02841, Republic of Korea.

E-mail addresses: seungja.oh@khu.ac.kr (S.J. Oh),

dupong76@korea.ac.kr (S.-W. Hwang).

¹ These authors contributed equally.

of wounds or accelerate the wound healing process through enhancement of angiogenesis and blood vessel formation [27,28]. Although previous reports described advances in materials science and sensing technology, certain research realms still remain unexplored; for example, electronic detection of biomolecules triggered in response to infection; and a wireless system integrated with sensing and therapeutic components.

Here, we introduce a flexible, wireless electronic wound dressing system that provides an all-in-one solution capable of simultaneously monitoring inflammatory (i.e., cathepsin) and physiological (humidity, pH, and temperature) biomarkers in wound beds, as well as biophysical therapy via electrical/optical treatments. Integration of electronics (planar capacitors and photodetectors) with a synthesized hydrogel, designed to structurally respond to cathepsin, provides a quantitative indication of inflammation caused by skin infection through external stimuli (e.g., bacteria, viruses, fungi). Wireless measurements of pathophysiological wound status and associated environments may provide the basis for an improved, quantitative approach to assess chronic risk and notify the need for further medical intervention, while tunable stimulation facilitates active treatments to improve tissue recovery during the healing process. In-depth *in vivo* investigations in living models demonstrate the overall capabilities for advanced wound management.

Soft, wireless electronic dressing system for wound healing

Fig. 1a presents exploded view illustration of an electronic wound dressing system that combines a conventional passive dressing with optoelectronic components capable of monitoring and healing the affected skin. The proposed system consists of two different layered units: (i) a disposable, skin-integrated unit (Unit I) contains arrays of biosensors for real-time monitoring of wound-related vital signs such as inflammation (cathepsin) and physiologies (humidity, pH, and temperature), as well as planar electrodes and optical sources for electrical/optical stimulations to accelerate wound healing; (ii) integrated electronic modules (Unit II) for remote control operation via a wireless link. Each unit can be simply assembled/disassembled via magnetic buttons and electrically connected/disconnected through a plug and play interface. The lower frame of Fig. 1a highlights the ability to observe concentrations of cathepsin – a biomarker strongly related to inflammatory responses – at wound sites, by a synthesized hydrogel designed to be cleaved in response to cathepsin release. Details of the material and reaction mechanism will be described in the following section. An optical image in Fig. 1b shows a representative device placed on a wound replica, which contains signal processors, Bluetooth module and a small rechargeable battery on a thin, flexible printed circuit board (FPCB). Fig. 1c presents an overall process diagram. Measured diverse parameters from Unit I were converted through sequential processing using amplifiers (AMP) and analog-to-digital converters (ADC), and transmitted through Bluetooth Low Energy (BLE) chip to external acquisition devices (shaded by red). The preprogrammed microcontroller and timer circuits in Unit II generated desired stimulation signals that were delivered to the electrical/optical components in Unit I (shaded by blue). Fig. 1d provides an example of application procedures of the electronic wound dressing on the skin, showing placement of Unit I, integration of Unit II, and wireless network operation using a smartphone-based application. Comparisons of features with previously reported wound systems is presented in Table S1.

Characterizations and analyses of inflammation-responsive hydrogels

Fig. 2a presents an image of inflammation-responsive gel (IFRep gel) that is composed of Norbornene-conjugated alginate backbones

cross-linked with peptides that can be cleaved by cathepsins. A series of illustrations in Fig. 2b describe the sequential reactions in which the IFRep gels were disintegrated when cathepsins were released from skin wounds. Fluorescent and scanning electron microscope (SEM) images in Fig. 2c exhibit changes in the volume and microstructure of the IFRep gels when immersed in buffer solutions with different cathepsin concentrations closely related to actual wound environments [29]. As the concentration increased, clear differences in the volume and pore density/size were observed, while no activity occurred in cathepsin-free buffers. A three-dimensional view of the fluorescent images and quantitative analysis using IVIS spectrum are shown in Fig. S1. Measured relative weight profiles in Fig. 2d indicate similar behavior consistent with the results in Fig. 2c. Such volumetric, structural reactivity of the IFRep gels can be tuned at desired rates by adjusting the molecular ratio of cathepsin-cleavable bonds to backbone polymer, for potential applications such as inflammation-responsive drug release. A previous report investigated detailed characterization of IFRep gels, including mechanical properties, swelling ratios and biocompatibility [30]. To electrically evaluate cathepsins-relevant changes, we employed two different electrical and optical approaches. Fig. 2e describes the overall sensing mechanism that can measure changes in the volumetric capacitance of hydrogels using planar interdigitated electrodes (IDEs), through the interaction between cathepsin and the gel. Fig. 2f presents a linear response of planar capacitors ($V = 1$ V, $F = 1$ kHz) covered with different thicknesses of IFRep gels, resulting that measured capacitances were directly proportional to the thickness due to the rise in the effective relative permittivity [31]. In addition, we collected time-varying responses of capacitors with a constant thickness (~ 2 mm) of IFRep gels after immersion in solutions of various cathepsin concentrations, as shown in Fig. 2g. The output capacitances decreased as cathepsin concentrations increased as expected, and revealed that cathepsins as a protease were active during the first 24 h, then gradually decreased and saturated [32]. The other strategy in Fig. 2h is to utilize thickness-dependent IR reflectance at the surface of hydrogels. Fig. 2i shows current responses of a photosensor that consists of an infrared (IR) LED as a light source and a transistor as a photodetector, as a function of the thicknesses of IFRep gels. As the thickness of IFRep gels decreased, reflected IR intensity increased, which generated the current output of the phototransistor [33]. Detailed electrical characteristics of photosensors are shown in Fig. S2. Similar to the conditions applied to IDE, immersion in cathepsin-varying media induced a large volume changes of IFRep gels, resulting in significant increment of the current responses (Fig. 2j). Summarized output characteristics of both sensors responding to a wide range of cathepsin levels appears in Fig. S3.

Electrical characterizations of sensing components for monitoring wound-related physiologies

Fig. 3a presents sensing component arrays, including hygrometers, thermometers, and pH sensors, for real-time, continuous monitoring of physiologies associated with wound status, with a magnified view of individual devices in the inset. Hygrometers can be performed using capacitance changes between interdigitated electrodes (IDEs) to obtain humidity around wound areas, preventing unwanted scabs (which can lead to scar formation) caused by dryness or infection from wetness [34]. As moisture adsorbed on IDEs increased, capacitances increased as shown in Fig. 3b, due to a larger dielectric constant (ϵ_r , 80.4) of water vapor than those of air (~ 1) or polyimide substrate (~ 3) at room temperature [35]. Fig. 3c shows measured changes in open circuit potential (OCP) between electrodeposited polyaniline (PANi) as working electrodes and silver/silver chloride (Ag/AgCl) as reference electrodes when immersed in solutions with different pH levels. The pH-dependent variations of

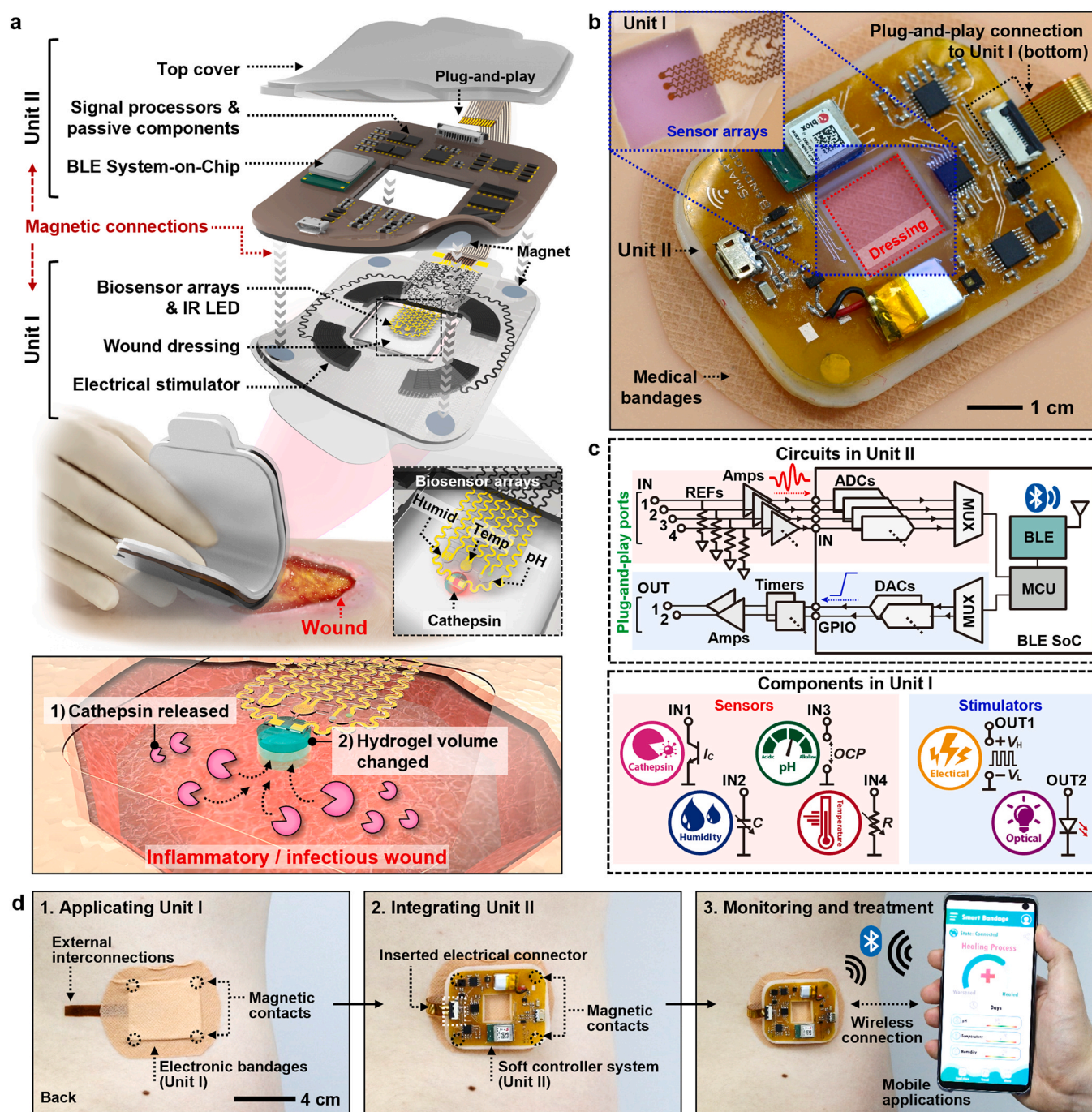


Fig. 1. Soft, wireless medical dressings integrated with electronic sensors and electrical/optical stimulators, for point-of-care of wounds. (a) Overall description of a proposed electronic/optical wound monitoring/healing system, consisting different layered units: (i) a disposable, skin-integrated unit (Unit I) that includes an array of monitoring components for vital signs of inflammation (i.e., cathepsin, CTS) and physiologies (i.e., humidity, pH, and temperature), as well as a light source and planar electrodes for sustained optical/electrical stimulations; (ii) a stand-alone electronic circuit (Unit II) for functional controls, measurements and wireless communication. Each unit can be assembled/disassembled via magnetic buttons and operated through plug and play interfaces. (b) Photograph of the whole system mounted onto a wound replica, with a magnified view of sensor arrays in Unit I. (c) Operational flow chart of the electronic system, including sensing elements, signal converters (e.g., photo-reflector, resonant driver, analog-to-digital converter, and voltage follower), wireless interfaces (i.e., Bluetooth low energy, BLE, unit), microcontrollers (MCU), and optical/electrical treatment components. (d) Sequential images of application procedures of the electronic bandage system for real-time and continuous access to patient's status via a smartphone-linked platform.

electrochemical potentials were caused by protonation/deprotonation in conjugated electronic structure, during exposure to acidic/basic environments [36]. This feature is very useful for tracking wound conditions since the pH of the skin varies, ranging from pH values of 4.0–6.0 (acidic) at normal, to ~ 7.4 (neutral) at an injured state, and to ~ 10.0 (basic) at infected wounds [37]. Fig. 3d shows distinct linear responses of arrays of thermometers over the range of

ambient to biological temperatures, enabling to provide temporal and spatial heat distribution associated with local blood flow, angiogenesis and fibrosis during the wound healing process [38]. Compared to a thermal image using a commercial infrared (IR) camera in Fig. 3e, a spatial temperature gradient obtained from the thermometer array exhibited similar range of properties as shown in Fig. 3f and S4. Such electrical fidelity was also confirmed using a

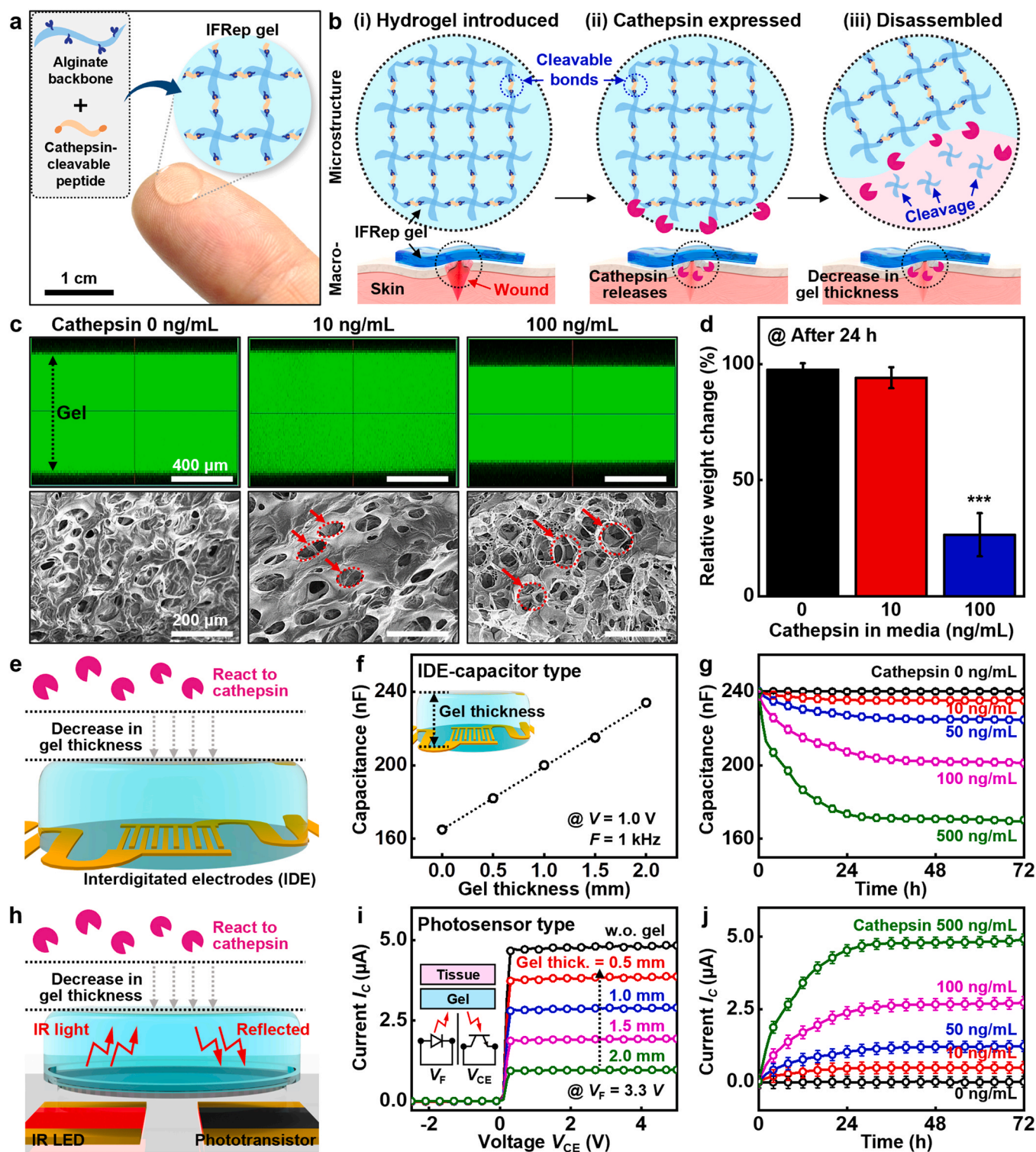


Fig. 2. Inflammation-responsive hydrogels (IFRep gel) integrated with electronic components for in situ monitoring of a wound infection. (a) Schematic illustration of an enzymatic reaction mechanism of IFRep gels under inflammatory conditions by cathepsins that cleave peptides in the hydrogel. (b) Optical images of an IFRep gel before and after gelation by ultraviolet (UV) exposure. (c) Fluorescent (top) and scanning electron microscope (SEM, bottom) images of IFRep gels immersed in buffer solutions with different cathepsin concentrations. (d) Relative weight change of IFRep gels 24 h after immersion in various cathepsin solutions. (e) Schematic of capacitive cathepsin detection using planar interdigitated electrodes (IDE) covered with IFRep gel. (f) Measured output capacitances depending on diverse thicknesses of IFRep gels, using interdigitated electrodes (IDEs) at the frequency of 1 kHz. (g) Time-varying changes in capacitance with different concentrations of cathepsins over 72 h. (h) An illustration of the photodetection of cathepsin using IR reflection. (i) Output current-voltage characteristics of a cathepsin photosensor consisting of IR LED and a phototransistor when covered with IFRep gels of different thicknesses. (j) Continuous measurements of electrical behaviors of photosensors when immersed in a wide range of cathepsin amounts over 72 h.

porcine skin under local temperature regulation (Fig. 3g). The performances of all the components are quite comparable to those of commercially available products (Fig. S5). Structural modifications

and configurations allowed the whole system to maintain stable operation against repeated external deformations, including bending and compressing modes in Fig. 3h.

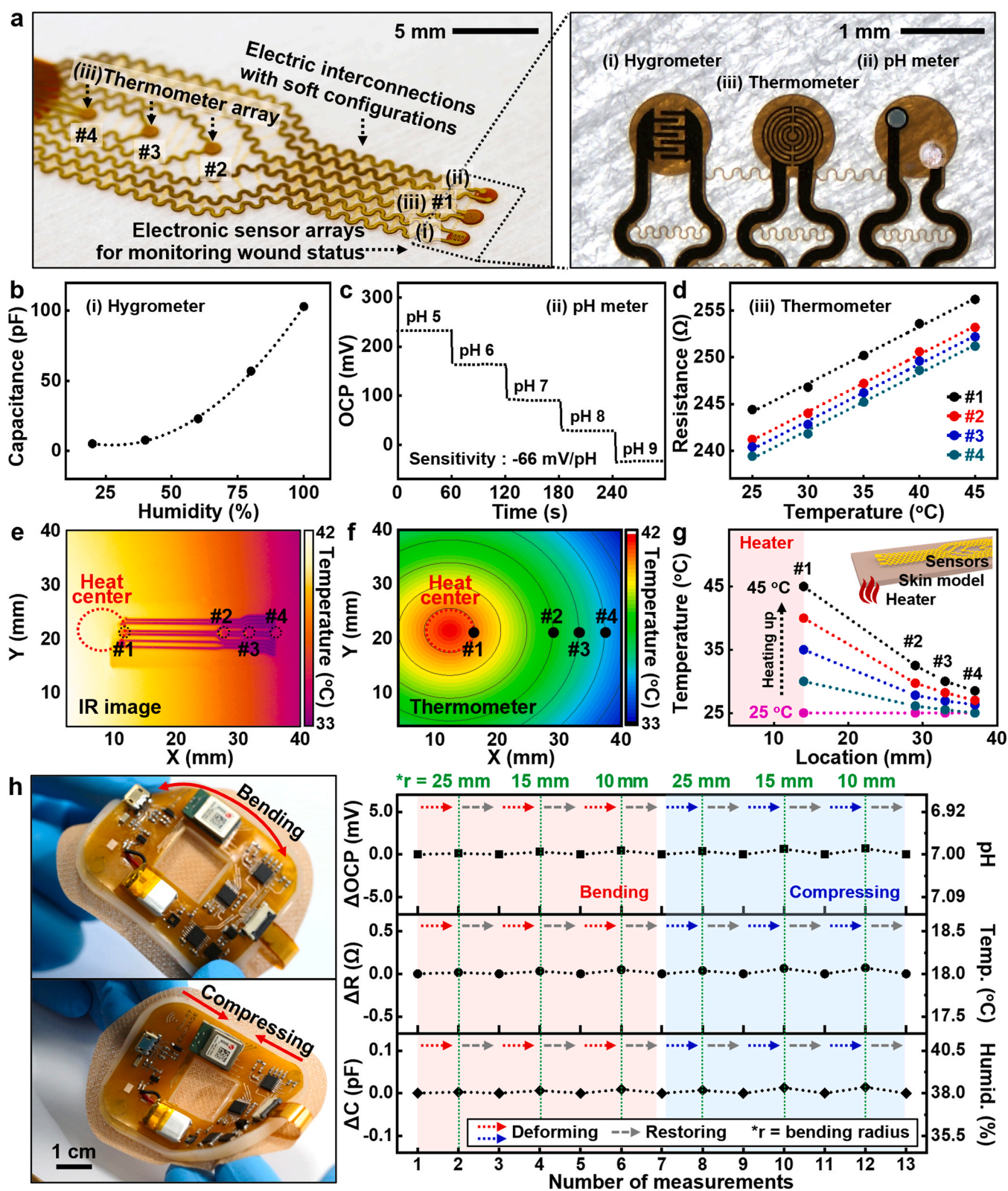


Fig. 3. Electrical characterizations of diverse biosensors for wound-related physiologies. (a) Optical images of sensor arrays, including hygrometer, pH meter, and thermometers, in a perspective view (left) and magnified view (right). (b) Measured capacitance changes of interdigitated electrodes (IDE)-based hygrometers in response to a wide range of humidity levels. (c) Temporal, continuous open circuit potential (OCP) responses of pH meters to buffer solutions of different pH ranges (pH 5 ~ 9). (d) Temperature-dependent changes in resistance of individual temperature sensors in arrays. (e) Infrared (IR) thermogram displaying uniform heat distribution around a heat source. (f) Corresponding spatial temperature gradient collected by an array of thermometers placed in each position (#1 ~ #4). (g) Measured spatial temperature distribution during heating to mimic the local temperature rise of the wound, in a porcine skin model with similar thermal conductivity and structure to the human skin. (h) Photographs (left) and relevant cyclic behaviors (right) during various deformations, for mechanically robust, reliable properties of each electronic component.

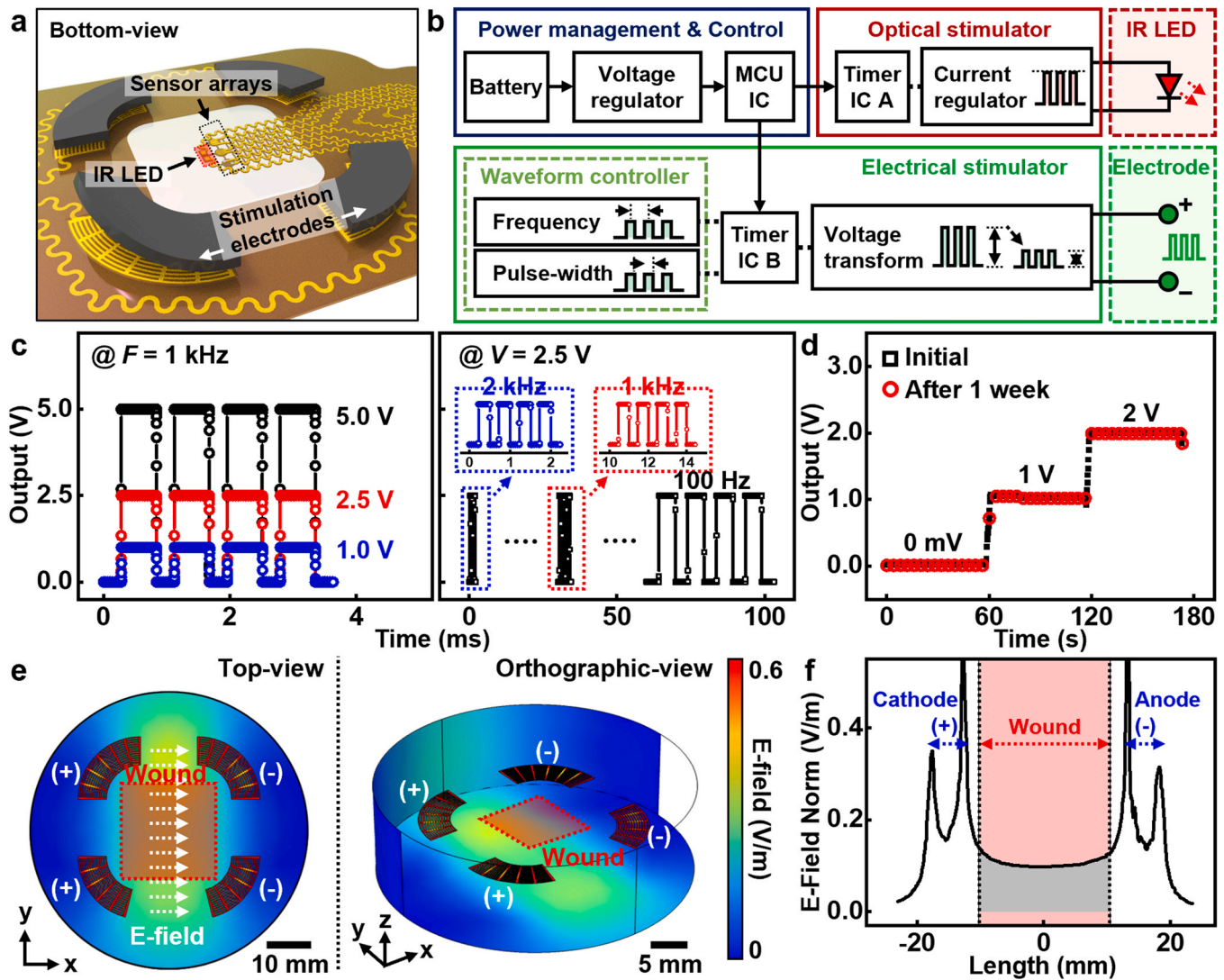
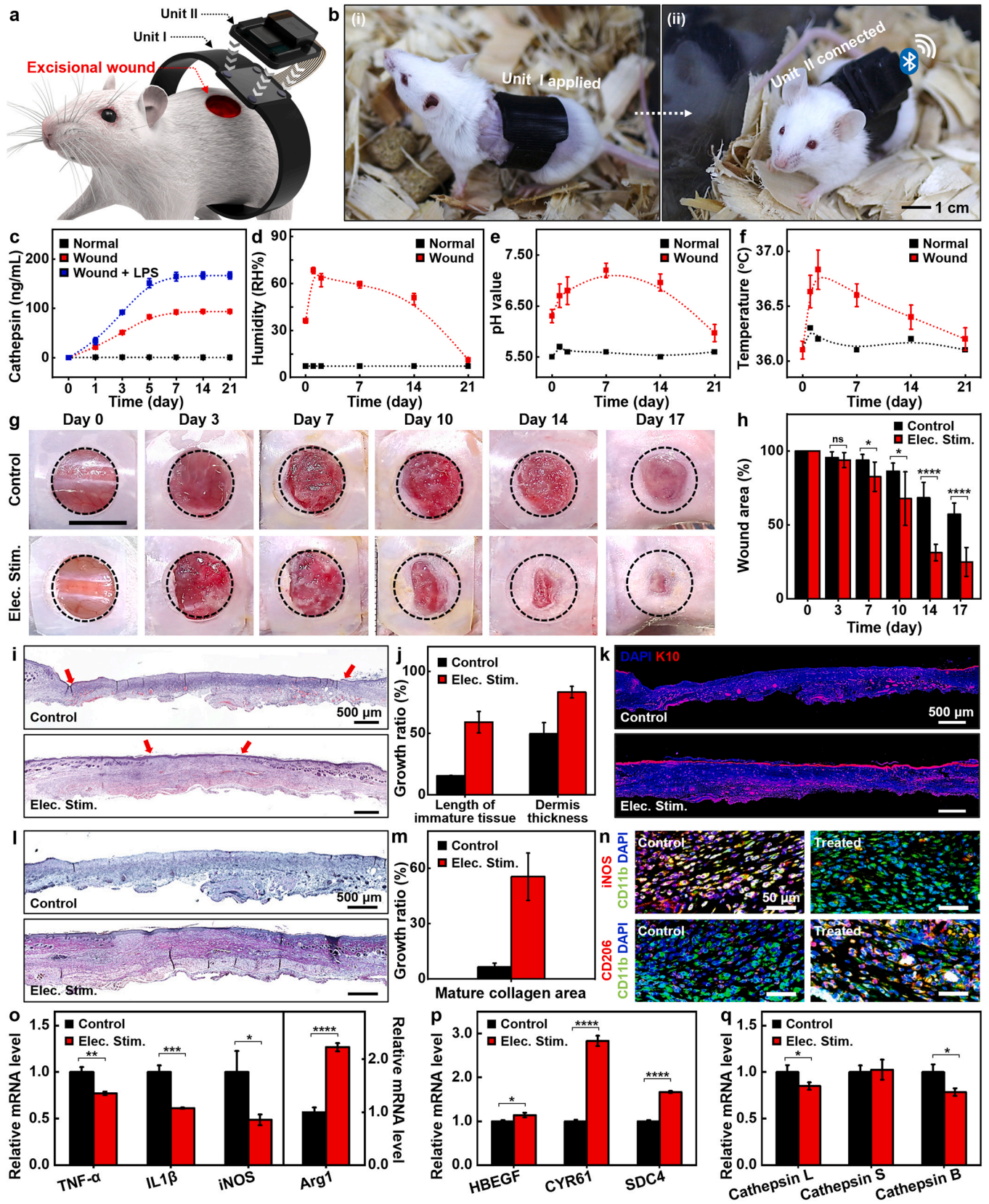


Fig. 4. Measured and simulated characteristics of active treatment systems for accelerating healing process. (a) Schematic description of electrical/optical stimulators integrated with sensor arrays. (b) Operational block diagram of the overall stimulation system, including power-managing parts, signal pulse and pattern generators, regulating and transforming components, and stimulation sources (light-emitting diodes (LED) and electrodes). (c) Output characteristics of rectangular waveforms generated by electrical stimulators, capable of varying amplitudes in a range of 1–5 V at a frequency of 1 kHz (left) and frequencies of 0.1–2 kHz with an applied voltage of 2.5 V (right). Insets show output signals in magnified timescales. (d) Durable output potentials at the initial state (black) and after 1 week of use (red). (e) Simulated results of electrical field (E-field) distribution induced by electrical stimulators around the wound area. (f) Uniform E-field profile at the wound site (shaded in gray) between cathodes (+) to anodes (-).

Various properties of electrical and optical stimulation systems

Fig. 4a illustrates an electrical, optical stimulator for accelerating the wound healing process, which soft, planar electrodes were attached to the skin around a wound for delivering electrical currents, and microscale near-infrared light-emitting diodes (μ -IRLEDs) were placed on the center of the wound to transport uniform photomodulation. Fig. 4b schematically presents a process flow of electronically controlled optical/electrical stimulators. Timer circuits in Fig. S6 provide specific square waveforms by adjusting frequency, pulse-width, and amplitude appropriate for use in biological tissues, under the controls of a microcontroller unit (MCU). Fig. 4c presents tunable characteristics of amplitude (left) and frequency (right) of a miniaturized pulse generator device. The stable voltage outputs of electrical stimulators were still maintained even after repeated daily use for a week on a porcine skin model (Fig. 4d), with negligible changes in electrodes impedance in Fig. S7. We also studied behaviors of the effective electric field (E-field) under given conditions

during electrical stimulations, by finite element analysis (FEA). A three-dimensional finite element wound-on-skin model was built with electrical properties in previous reports [39], and four quarter-ring-shaped electrodes were placed on the skin around the wound. Results revealed that the designed configuration can deliver uniform endogenous E-field in the wound area of 2 cm X 2 cm, as shown in Fig. 4e. Detailed information on simulation is presented in the Method section. Cross-sectional profiles of E-field in Fig. 4f and S8 show that the effective lateral E-field in the wound region was approximately ~ 0.1 V/m while applying 3 V to cathodes (+) against grounded anodes (-). Such value is quite comparable to that of physiologically relevant electric fields to activate the migration of epithelial cells during the wound healing process [27,28]. Photothermal therapy is also possible in a similar way, yet it requires careful understanding and control of the intensity and wavelength of light. A thermographic image in Fig. S9a shows local IR radiation of a phototherapeutic device before and after applying a voltage (2 V). Fig. S9b provides current-voltage (I-V) characteristics of a μ -IRLED



(caption on next page)

Fig. 5. *In vivo* evaluations of integrated wound dressing systems for on-demand electrical treatments and real-time monitoring. (a) Description of a soft, wireless electronic wound dressing system in a miniaturized form for biological models. (b) Photographs of a Unit I containing sensors and stimulation electrodes on a mouse dorsal wound (i), and of an assembled Unit II for functional controls, measurements, and wireless communication (ii). (c) Measured various cathepsin levels in normal skins (black), wounds (red), and lipopolysaccharide (LPS)-loaded wounds (blue) for 3 weeks. (d) Recorded rise and fall in humidity (i.e., moisture) levels at injured sites relying on various wound stages. (e) Collected variations of pH values at the naturally acidic outer skin (normal), compared to the neutral environments of wounds (wound). (f) Continuous measurement of changes in temperature at wound sites during the healing process. (g) Representative images of wound closure without or with electric stimulation at each time point for 17 days (Scale bar, 10 mm). (h) The wound closure (%) at each time point for 17 days. (i) Images of H&E staining of wound section at day 17 (red arrow, the wound edges). (j) Comparisons of the length of immature tissue (left) and the thickness of regenerated dermal tissue (right) after 17 days from H&E-stained images of control (black) and electrical stimulation groups (red). (k) Images of immunofluorescence staining with cytokeratin 10 at day 17. (l) Images of Herovici staining of wound section at day 17. (m) Deposition of mature collagen area in wound area of Herovici stained images. (n) Immunofluorescence staining of M1 (CD11b⁺iNOS⁺ cells) and M2 (CD11b⁺CD206⁺ cells) markers. (o–q) Relative mRNA levels of inflammatory (o, left), anti-inflammatory (o, right), keratinocyte activation (p), and cathepsin markers (q).

with a specific wavelength of 850 nm in Fig. S9c, which can produce biologically positive effects such as fibroblast proliferation and collagen synthesis [27,28].

In Vivo demonstrations of electronic wound dressing systems

Fig. 5a shows a soft, miniaturized electronic wound dressing system, allowing for determination of biochemical and physiological conditions at affected regions and for stimulations to hasten wound healing in living models. Full-thickness excisional wounds (~10 mm in diameter) were created using a medical-grade biopsy punch on the dorsum of mice, to evaluate the capabilities of devices. Detailed surgical procedures appear in the Method section. Photographs in Fig. 5b show brief, sequential steps to apply Unit I onto the excisional wound and combine Unit II to form a complete system. Fig. 5c–f summarizes the results of comprehensive 21-day monitoring of relevant parameters, including cathepsin (Fig. 5c), humidity (Fig. 5d), pH (Fig. 5e), and temperature (Fig. 5f), compared to the normal skin in the same model. Levels of cathepsin, an inflammation-related biomarker, increased in skin wounds during the first 5 days, while remained unchanged in the control group (normal, Fig. 5c). During the same period, excessively elevated levels of cathepsin were monitored when injection with lipopolysaccharide (LPS), a pathogenic stimulator from *Klebsiella pneumonia* that mimics a bacterial infection wound model [40–42]. The results demonstrate the ability to detect abnormal ranges of cathepsin concentration, which can be a means of appropriate medical precautions and treatments to prevent unexpected infections from developing into a critical condition. The addition of reversible functions such as self-healing or re-crosslinkable to the hydrogel design can further obtain dynamic biochemical signals and even repeated changes [43]. Moisture balance is a key factor in acute and chronic wound care since a moist environment accelerates wound healing rates and promotes cellular growth, angiogenesis and epithelialization [34,44]. Fig. 5d provides measured changes in humidity that rapidly increased at the initial stage due to wound exudate as a normal healing process, remained within an adequate moist range, and tended to gradually decrease to a normal level with the healing process [34]. The collected results in Fig. 5e present temporal behaviors of pH scales. The value at the early stage increased to 7.4, higher than a healthy skin pH (4.0–6.0) because of internal tissue exposure and outflow of interstitial fluids, and then decreased as healed [37,45]. Fig. 5f exhibits variations of temperature at wound sites over the process of wound healing. As compared to normal skin, initial rises in temperature at damaged regions were due to local blood flow, potentially associated with induced angiogenesis and fibrosis (Fig. S10) [38,46].

To investigate *in vivo* efficacy of electrical stimulation for accelerating the wound healing process, a full-thickness wound was treated with the electronic device ($V = 2.5$ V, $F = 1$ kHz) for 17 days. A collected set of pictures in Fig. 5g present evaluation of wound healing rates for each group with/without electrical stimulation, resulting that electrotherapy was clearly effective after day 10, which

was supported by quantitative analysis of wound closure between the electrically treated group ($75 \pm 9.8\%$) and the control group ($43 \pm 7.5\%$) (Fig. 5h). Histological analysis via H&E staining in Fig. 5i–j revealed that the length of immature tissue (re-epithelialization) and total dermal thickness were improved in the treated group. For the detailed analysis of epidermis formation, immunofluorescence staining of cytokeratin 10 (K10) was performed to confirm keratinocyte distribution in the wound site (Fig. 5k). As a result, the epidermis formation was promoted in the stimulated group. In addition, the electrical stimulation enhanced mature collagen deposition in the wound bed as indicated by the red color of Herovici staining in Fig. 5l as well as quantitative counts in Fig. 5m. To evaluate the immunomodulatory effect of the electrical stimulation, we examined the expression of pro- and anti-inflammatory markers in the wound site. The co-staining of inflammatory marker, inducible nitric oxide synthase (iNOS), and macrophage marker (CD11b), indicating M1 macrophages, was significantly suppressed on day 17 in the treated group (Fig. 5n (top)). On the other hand, the co-staining of anti-inflammatory marker (CD206) and macrophage marker (CD11b), indicating M2 macrophages, was remarkably increased in the treated group compared to the control group (Fig. 5n (bottom)). In addition, mRNA levels of inflammatory genes, including TNF- α , IL-1 β , and iNOS, were effectively suppressed whereas mRNA levels of the anti-inflammatory gene, Arg1, were significantly upregulated in the treated group (Fig. 5o). The mRNA levels of keratinocyte activation markers (HBEGF, CYR61, SDC4) inducing wound remodeling were also increased in the treated group (Fig. 5p). Collectively, the electrical stimulation successfully accelerated wound healing by triggering keratinocytes and fibroblasts migration [47]. The expression levels of cathepsin, in particular, L and B which are indicators of the inflammatory environment was decreased in the treated group (Fig. 5q), showing the stimulation attenuated the inflammatory response inducing the wound remodeling phase, which is the important transition in the wound healing process [48,49]. The overall results indicate the electronic dressing devices induced wound healing acceleration without any adverse effects during the recovery period.

Conclusions

The concepts, materials, devices, and system integration approaches reported here suggested a soft, wireless dressing system for use in wounds. The comprehensive results represent the feasibility of skin-integrated electronics, which not only monitor vital signs, including cathepsin levels (as a wound inflammatory marker), humidity, pH, and temperature, to analyze physiological wound status but also provide appropriate treatments using electrical and optical stimulation to improve wound healing rate. Based on the monitored wound condition, precise on-demand treatment can be further realized. Fully wireless operation modes with animal models offer a systematic tool for point-of-care and nurse-free management of skin wounds, accessible outside the clinical setting.

Materials and methods

Fabrication of cathepsins-responsive hydrogel

The cathepsins-responsive hydrogel was fabricated as in the previous study [30]. In brief, alginate (PRONOVA UP) was conjugated with 5-norbornene-2-methylamine using ethyl(dimethylamino-propyl)carbodiimide/N-hydroxysuccinimide (EDC/NHS) synthesis and the reaction was kept at room temperature for 24 h. After the reaction, the solution was dialyzed with NaCl solutions in deionized water (DI) for 3 days. Norbornene-conjugated alginate (Nor_Al) solution was sterilized with a 0.22 μm filter and lyophilized for 2 days. For the study, 2.5 wt% Nor_Al with Irgacure was added to the mold, followed by cathepsin cleavage crosslinking agent (CARLRC) at a concentration of 4 mM. Finally, the mixture of solutions was exposed to UV light (365 nm, 10 mW/cm²) for 10 min

Fabrication of electronic wound dressing systems

Fabrication began with preparation of a polyimide (PI) film (25 μm thick) onto a PDMS-coated glass slide. A thin metal bilayer of chromium/gold (Cr/Au, 10/200 nm thick) on the PI substrates was deposited via an electron-beam (E-beam) evaporator, followed by photolithographic patterning and wet etching procedures to define desired geometries, including cathepsin analyzers, interdental humidity meters, electrochemical pH electrodes, meander-shaped resistive thermometers, electrical/optical stimulators and interconnections. A spin-coated PI layer with patterned openings via dry etching, covered metal traces except for wound-faced sensing/stimulating regions. Electrochemical depositions formed pH-active polyaniline (PANI) layer via cyclic voltammetry (CV) with sweeping of -0.2 – 1.0 V versus a commercial reference electrode (Ag/AgCl) at a scan rate of 100 mV/s, during immersed in 0.1 M aniline (Sigma-Aldrich, USA) in 1 M HCl (Sigma-Aldrich, USA) aqueous solution. Ag/AgCl ink (ALS, Japan) was printed on the desired area of Au electrodes using a stencil mask and then dried on a hotplate at 120 °C for 5 min to create a reference electrode. A commercial photo-interrupter chip (SHARP, Japan) composed of an infrared (IR) light-emitting diode (LED) and a phototransistor was integrated with other components, and subsequently covered with an inflammation-responsive hydrogel to complete the fabrication of cathepsin phototensors.

Fabrication and assembly of soft wireless electronic systems

Schematic design and printed circuit board (PCB) layouts of electronic systems were achieved using a commercial electronic design automation (EDA) software (EAGLE, Autodesk, USA). Conventional flexible printed circuit board (FPCB) fabrication procedures, including photolithography, etching and electroplating process, provided desired geometries of conductive traces in circuits. A Bluetooth 5 Low Energy (BLE) module (NINA-B306, Nordic Semiconductor, USA), analog-to-digital converters (ADS1219, Texas Instruments, USA), NE555 timers, magnet buttons, and commercial passive components that include connectors, capacitors, inductors, and resistors were assembled on prepared footprints. Soft silicone rubbers were cured in 3D-printed mold and served as encapsulations and housing cases.

Evaluation of wound healing effect using in vivo full-thickness wound models

The animal study was approved by Korea Institute of Science and Technology (KIST-2021-11-147). All animal experiments were performed according to the International Guide for the Care and Use of Laboratory Animals. For in vivo wound model, Balb/c mice (male, 6

weeks, Orient Bio, Korea) were used after an acclimation period of 1 week. Before surgery, mice were anesthetized by isoflurane in oxygen, and the hair was removed using a clipper. After sterilizing with an alcohol gauze, the 10 mm full-thickness wound was made using a biopsy punch on a dorsal skin. The silicon splinting ring (0.5 mm-thickness) was glued and sutured around the wound, and then the electronic system was introduced onto the wound. Arduino IDE (Arduino LLC, Italy) software programmed operations of micro-controllers in electronic systems and custom LabVIEW software (National Instruments, USA) acquired electrically measured data. Measurements and stimulation were performed daily in awake, freely moving models with limited anesthesia, except for dressing replacements, to minimize anesthesia-induced deterioration in recovery. For in vivo real-time monitoring, a bacterial infectious wound model was developed using LPS derived from *Klebsiella pneumonia* (Sigma, #L4268). 10 μg of LPS was injected into the 10 mm full-thickness wound bed.

Histology

The collected sample was fixed with 10% formalin and immersed in a paraffin block. Tissue blocks were sectioned into 4 μm -thickness slices and sequentially deparaffinized and hydrated by treatment with xylene and ethanol solutions, respectively. Slices were stained with hematoxylin and eosin staining (H&E) and Herovici staining and observed under an optical microscope.

Immunofluorescent staining

For immunofluorescence staining of in vivo tissue sectioned slices, CD11b (Biolegend, #101201), iNOS (Millipore, #06-573), CD206 (#ab64693), cytokeratin 10 (#ab76318) were used for primary antibodies, and the secondary antibodies Rabbit IgG (Invitrogen, #A21207) and Goat anti-Mouse IgG (Invitrogen, #A11001) were used. The immunostained section was observed by a confocal microscope (Carl Zeiss).

Author's contribution

S.M.Y., H.K., and G.-J.K. contributed equally to this paper.

Notes

The authors declare no competing financial interest.

CRedit authorship contribution statement

Seung Min Yang: Conceptualization, Formal analysis, Investigation, Writing – original draft, Visualization. **Hyerim Kim:** Methodology, Formal analysis, Investigation, Writing – original draft. **Gwan-Jin Ko:** Methodology, Formal analysis, Investigation, Writing – original draft. **Jong Chan Choe:** Methodology, Validation, Investigation. **Joong Hoon Lee:** Methodology, Investigation, Visualization. **Kaveti Rajaram:** Software, Validation, Formal analysis. **Byoung-ha An:** Validation, Resources. **Won-Bae Han:** Investigation. **Dong-Je Kim:** Validation. **Jeong-Woong Shin:** Validation. **Tae-Min Jang:** Investigation. **Heeseok Kang:** Validation. **Sungkeun Han:** Validation. **Kangwon Lee:** Supervision. **Seung Ja Oh:** Supervision, Resources, Funding acquisition; **Suk-Won Hwang:** Supervision, Writing – review & editing, Funding acquisition.

Data Availability

The data that has been used is confidential.

Declaration of Competing Interest

The authors declare that they have no known competing financial interests or personal relationships that could have appeared to influence the work reported in this paper.

Acknowledgments

This work was supported by a Korea University grant, KU-KIST Graduate School of Converging Science and Technology Program, National Research Foundation of Korea (NRF) grant funded by the Korea government (the Ministry of Science and ICT, MSIT) (grant NRF-2017R1E1A1A01075027, 2020R1C1C1009507, RS-2022-00165524), the Korea Medical Device Development Fund Grant funded by the Korea Government (the Ministry of Science and ICT, the Ministry of Trade, Industry & Energy, the Ministry of Health & Welfare, and the Ministry of Food and Drug Safety) (1711174536, RS-2020-KD000138), the Ministry of the Science and ICT (MSIT), under the ICT Creative Consilience program (IITP-2022-2020-0-01819) supervised by the IITP (Institute for Information & communications Technology Planning & Evaluation), and the KIST Institutional Program to S.J.O.

Appendix A. Supporting information

Supplementary data associated with this article can be found in the online version at doi:10.1016/j.nantod.2022.101685.

References

- [1] B. Wang, C. Zhao, Z. Wang, K.A. Yang, X. Cheng, W. Liu, W. Yu, S. Lin, Y. Zhao, K.M. Cheung, H. Lin, H. Hoiyai, P.S. Weiss, M.N. Stojanović, A.J. Tomiyama, A.M. Andrews, S. Emaminejad, Wearable aptamer-field-effect transistor sensing system for noninvasive cortisol monitoring, *Sci. Adv.* 8 (2022) abk0967.
- [2] Y. Zhao, B. Wang, H. Hoiyai, Z. Wang, S. Lin, C. Yeung, H. Lin, P. Nguyen, K. Chiu, K. Salahi, X. Cheng, J. Tan, B.A. Cerrillos, S. Emaminejad, A wearable freestanding electrochemical sensing system, *Sci. Adv.* (6) (2020) aaz0007.
- [3] S.M. Yang, J.H. Shim, H.-U. Cho, T.-M. Jang, G.-J. Ko, J. Shim, T.H. Kim, J. Zhu, S. Park, Y.S. Kim, S.-Y. Joong, J.C. Choe, J.-W. Shin, J.H. Lee, Y.M. Kang, H. Cheng, Y. Jung, C.-H. Lee, D.P. Jang, S.-W. Hwang, Hetero-integration of silicon nanomembranes with 2D materials for bioresorbable, wireless neurochemical system, *Adv. Mater.* 34 (2022) 2108203.
- [4] J.H. Lee, H. Kim, J.-Y. Hwang, J. Chung, T.-M. Jang, D.G. Seo, Y. Gao, J. Lee, H. Park, S. Lee, H.C. Moon, H. Cheng, S.-H. Lee, S.-W. Hwang, 3D printed, customizable, and multifunctional smart electronic eyeglasses for wearable healthcare systems and human-machine interfaces, *ACS Appl. Mater. Interfaces* 12 (2020) 21424–21432.
- [5] D. Jung, C. Lim, H.J. Shim, Y. Kim, C. Park, J. Jung, S.I. Han, S.H. Sunwoo, K.W. Cho, G.D. Cha, D.C. Kim, J.H. Koo, J.H. Kim, T. Hyeon, D.-H. Kim, Highly conductive and elastic nanomembrane for skin electronics, *Science* 373 (2021) 1022–1026.
- [6] Z. Rao, Y. Lu, Z. Li, K. Sim, Z. Ma, J. Xiao, C. Yu, Curvy, shape-adaptive imagers based on printed optoelectronic pixels with a kirigami design, *Nat. Electron.* 4 (2021) 513–521.
- [7] M. Baumgartner, F. Hartmann, M. Drack, D. Preninger, D. Wirthl, R. Gerstmayr, L. Lehner, G. Mao, R. Pruckner, S. Demchyshyn, L. Reiter, M. Strobel, T. Stockinger, D. Schiller, S. Kimeswenger, F. Greibich, G. Buchberger, E. Bradt, S. Hild, S. Bauer, M. Kaltenbrunner, Resilient yet entirely degradable gelatin-based biogels for soft robots and electronics, *Nat. Mater.* 19 (2020) 1102–1109.
- [8] Y.S. Oh, J.H. Kim, Z. Xie, S. Cho, H. Han, S.W. Jeon, M. Park, M. Namkoong, R. Avila, Z. Song, S.U. Lee, K. Ko, J. Lee, J.S. Lee, W.G. Min, B.J. Lee, M. Choi, H.U. Chung, J. Kim, M. Han, J. Koo, Y.S. Choi, S.S. Kwak, S.B. Kim, J. Kim, J. Choi, C.M. Kang, J.U. Kim, K. Kwon, S.M. Won, J.M. Baek, Y. Lee, S.Y. Kim, W. Lu, A. Vazquez-Guardado, H. Jeong, H. Ryu, G. Lee, K. Kim, S. Kim, M.S. Kim, J. Choi, D.Y. Choi, Q. Yang, H. Zhao, W. Bai, H. Jang, Y. Yu, J. Lim, X. Guo, B.H. Kim, S. Jeon, C. Davies, A. Banks, H.J. Sung, Y. Huang, I. Park, J.A. Rogers, Battery-free, wireless soft sensors for continuous multi-site measurements of pressure and temperature from patients at risk for pressure injuries, *Nat. Commun.* 12 (2021) 5008.
- [9] K. Sim, F. Ershad, Y. Zhang, P. Yang, H. Shim, Z. Rao, Y. Lu, A. Thukral, A. Elgalad, Y. Xi, B. Tian, D.A. Taylor, C. Yu, An epicardial bioelectronic patch made from soft rubbery materials and capable of spatiotemporal mapping of electrophysiological activity, *Nat. Electron.* 3 (2020) 775–784.
- [10] Y.S. Choi, R.T. Yin, A. Pfenniger, J. Koo, R. Avila, K. Benjamin Lee, S.W. Chen, G. Lee, G. Li, Y. Qiao, A. Murillo-Berlitz, A. Kiss, S. Han, S.M. Lee, C. Li, Z. Xie, Y.Y. Chen, A. Burrell, B. Geist, H. Jeong, J. Kim, H.J. Yoon, A. Banks, S.K. Kang, Z.J. Zhang, C.R. Haney, A.V. Sahakian, D. Johnson, T. Efimova, Y. Huang, G.D. Trachiotis, B.P. Knight, R.K. Arora, I.R. Efimov, J.A. Rogers, Fully implantable and bioresorbable cardiac pacemakers without leads or batteries, *Nat. Biotechnol.* 39 (2021) 1228–1238.
- [11] Y. Yang, M. Wu, A. Vázquez-Guardado, A.J. Wegener, J.G. Grajales-Reyes, Y. Deng, T. Wang, R. Avila, J.A. Moreno, S. Minkowicz, V. Dumrongprechachan, J. Lee, S. Zhang, A.A. Legaria, Y. Ma, S. Mehta, D. Franklin, L. Hartman, W. Bai, M. Han, H. Zhao, W. Lu, Y. Yu, X. Sheng, A. Banks, X. Yu, Z.R. Donaldson, R.W. Gereau, C.H. Good, Z. Xie, Y. Huang, Y. Kozorovitskiy, J.A. Rogers, Wireless multilateral devices for optogenetic studies of individual and social behaviors, *Nat. Neurosci.* 24 (2021) 1035–1045.
- [12] G.-J. Ko, S.D. Han, J.-K. Kim, J. Zhu, W.B. Han, J. Chung, S.M. Yang, H. Cheng, D.-H. Kim, C.-Y. Kang, S.-W. Hwang, Biodegradable, flexible silicon nanomembrane-based NOx gas sensor system with record-high performance for transient environmental monitors and medical implants, *NPG Asia Mater.* 12 (2020) 71.
- [13] H. Jeong, J.Y. Lee, K.H. Lee, Y.J. Kang, J.T. Kim, R. Avila, A. Tzavelis, J. Kim, H. Ryu, S.S. Kwak, J.U. Kim, A. Banks, H. Jang, J.K. Chang, S. Li, C.K. Mummidisetty, Y. Park, S. Nappi, K.S. Chun, Y.J. Lee, K. Kwon, X. Ni, H.U. Chung, H. Luan, J.H. Kim, C. Wu, S. Xu, A. Banks, A. Jayaraman, Y. Huang, J.A. Rogers, Differential cardiopulmonary monitoring system for artifact-canceled physiological tracking of athletes, workers, and COVID-19 patients, *Sci. Adv.* 7 (2021) eabg3092.
- [14] T. Stockinger, D. Wirthl, G. Mao, M. Drack, R. Pruckner, S. Demchyshyn, M. Steiner, F. Egger, U. Müller, R. Schwödauer, S. Bauer, N. Arnold, M. Kaltenbrunner, iSens: a fiber-based, highly permeable and imperceptible sensor design, *Adv. Mater.* 33 (2021) 2102736.
- [15] X. Yu, Z. Xie, Y. Yu, J. Lee, A. Vazquez-Guardado, H. Luan, J. Ruban, X. Ning, A. Akhtar, D. Li, B. Ji, Y. Liu, R. Sun, J. Cao, Q. Huo, Y. Zhong, C.M. Lee, S.Y. Kim, P. Gutruf, C. Zhang, Y. Xue, Q. Guo, A. Chempakasseril, P. Tian, W. Lu, J.Y. Jeong, Y.J. Yu, J. Cormman, C.S. Tan, B.H. Kim, K.H. Lee, X. Feng, Y. Huang, J.A. Rogers, Skin-integrated wireless haptic interfaces for virtual and augmented reality, *Nature* 575 (2019) 473–479.
- [16] T.-M. Jang, J.H. Lee, H. Zhou, J. Joo, B.H. Lim, H. Cheng, S.H. Kim, I.-S. Kang, K.-S. Lee, E. Park, S.-W. Hwang, Expandable and implantable bioelectronic complex for analyzing and regulating real-time activity of the urinary bladder, *Sci. Adv.* 6 (2020) eabc9675.
- [17] R. Parameswaran, K. Koehler, M.Y. Rotenberg, M.J. Burke, J. Kim, K.Y. Jeong, B. Hissa, M.D. Paul, K. Moreno, N. Sarma, T. Hayes, E. Sudzilovsky, H.G. Park, B. Tian, Optical stimulation of cardiac cells with a polymer-supported silicon nanowire matrix, *Proc. Natl. Acad. Sci. U. S. A.* 116 (2019) 413–421.
- [18] J. Lee, H.R. Cho, G.D. Cha, H. Seo, S. Lee, C.-K. Park, J.W. Kim, S. Qiao, L. Wang, D. Kang, T. Kang, T. Ichikawa, J. Kim, H. Lee, W. Lee, S. Kim, S.-T. Lee, N. Lu, T. Hyeon, S.H. Choi, D.-H. Kim, Flexible, sticky, and biodegradable wireless device for drug delivery to brain tumors, *Nat. Commun.* 10 (2019) 5205.
- [19] H. Joo, Y. Lee, J. Kim, J.S. Yoo, S. Yoo, S. Kim, A.K. Arya, S. Kim, S.H. Choi, N. Lu, H.S. Lee, S. Kim, S.T. Lee, D.H. Kim, Soft implantable drug delivery device integrated wirelessly with wearable devices to treat fatal seizures, *Sci. Adv.* 7 (2021) eabd4639.
- [20] Y. Lee, T. Kang, H.R. Cho, G.J. Lee, O.K. Park, S. Kim, B. Lee, H.M. Kim, G.D. Cha, Y. Shin, W. Lee, M. Kim, H. Kim, Y.M. Song, S.H. Choi, T. Hyeon, D. Kim, Localized delivery of theranostic nanoparticles and high-energy photons using micro-needles-on-bioelectronics, *Adv. Mater.* 33 (2021) 2100425.
- [21] H. Seo, S.I. Han, K. Song, D. Seong, K. Lee, S.H. Kim, T. Park, J.H. Koo, M. Shin, H.W. Baac, O.K. Park, S.J. Oh, H. Han, H. Jeon, Y. Kim, D. Kim, T. Hyeon, D. Son, Durable and fatigue-resistant soft peripheral neuroprosthetics for in vivo bidirectional signaling, *Adv. Mater.* 33 (2021) 2007346.
- [22] Z. Xiong, S. Achavananthadith, S. Lian, L. Edward Madden, Z.X. Ong, W. Chua, V. Kalidasan, Z. Li, Z. Liu, P. Singh, H. Yang, S.P. Heussler, S.M.P. Kalaiselvi, M.B.H. Breese, H. Yao, Y. Gao, K. Sanmugam, B.C.K. Tee, P.Y. Chen, W. Loke, C.T. Lim, G.S.H. Chiang, B.Y. Tan, H. Li, D.L. Becker, J.S. Ho, A wireless and battery-free wound infection sensor based on DNA hydrogel, *Sci. Adv.* 7 (2021) eabj1617.
- [23] Y. Gao, D.T. Nguyen, T. Yeo, S. Bin Lim, W.X. Tan, L.E. Madden, L. Jin, J.Y. Kenan Long, F.A. Bakar Aloweni, Y.J. Angela Liew, M.L. Ling Tan, S.Y. Ang, S.D.O. Maniya, I. Abdelwahab, K.P. Loh, C.H. Chen, D.L. Becker, D. Leavelley, J.S. Ho, C.T. Lim, A flexible multiplexed immunosensor for point-of-care in situ wound monitoring, *Sci. Adv.* 7 (2021) eabg9614.
- [24] P. Kassal, J. Kim, R. Kumar, W.R. De Araujo, I.M. Steinberg, M.D. Steinberg, J. Wang, Smart bandage with wireless connectivity for uric acid biosensing as an indicator of wound status, *Electrochim. Commun.* 56 (2015) 6–10.
- [25] P. Mostafalu, A. Tamayol, R. Rahimi, M. Ochoa, A. Khalilpour, G. Kiaee, I.K. Yazdi, S. Bagherifard, M.R. Dokmeci, B. Ziaie, S.R. Sonkusale, A. Khademhosseini, Smart bandage for monitoring and treatment of chronic wounds, *Small* 14 (2018) 1703509.
- [26] Q. Pang, D. Lou, S. Li, G. Wang, B. Qiao, S. Dong, L. Ma, C. Gao, Z. Wu, Smart flexible electronics-integrated wound dressing for real-time monitoring and on-demand treatment of infected wounds, *Adv. Sci.* 7 (2020) 1902673.
- [27] J.M. McCulloch, L. Kloth, Kloth, Wound Healing: Evidence-based Management 19103 F. A. Davis Company, Philadelphia, PA, 2010.
- [28] M. Zhao, B. Song, J. Pu, T. Wada, B. Reid, G. Tai, F. Wang, A. Guo, P. Walczysko, Y. Gu, T. Sasaki, A. Suzuki, J.V. Forrester, H.R. Bourne, P.N. Devreotes, C.D. McCaig, J.M. Penninger, Electrical signals control wound healing through phosphatidylinositol-3-OH kinase-γ and PTEN, *Nature* 442 (2006) 457–460.
- [29] M. Abdul Latif, M. Zulasyraf Mohd Zaki, T. May Leng, N. Hidayah Abdul Rahman, S. Aisyah Arshad, A. Hamid, Alopecia denudata Engler treatment enhance open wound healing activities in Wistar rat's skin, *J. Ethnopharmacol.* 176 (2015) 258–267.
- [30] H. Kim, Y. Joo, Y.M. Kook, N.L. Tran, S.H. Kim, K. Lee, S.J. Oh, On-demand local immunomodulation via epigenetic control of macrophages using an

- inflammation-responsive hydrogel for accelerated wound healing, *ACS Appl. Mater. Interfaces* 14 (2022) 4931–4945.
- [31] H. Yuk, B. Lu, X. Zhao, Hydrogel bioelectronics, *Chem. Soc. Rev.* 48 (2019) 1642–1667.
- [32] F.A. Jaffer, D.E. Kim, L. Quinti, C.H. Tung, E. Aikawa, A.N. Pande, R.H. Kohler, G.P. Shi, P. Libby, R. Weissleder, Optical visualization of cathepsin K activity in atherosclerosis with a novel, protease-activatable fluorescence sensor, *Circulation* 115 (2007) 2292–2298.
- [33] C. McDonagh, C.S. Burke, B.D. MacCraith, Optical chemical sensors, *Chem. Rev.* 108 (2008) 400–422.
- [34] S.D. Milne, I. Seoudi, H. Al Hamad, T.K. Talal, A.A. Anoop, N. Allahverdi, Z. Zakaria, R. Menzies, P. Connolly, A wearable wound moisture sensor as an indicator for wound dressing change: an observational study of wound moisture and status, *Int. Wound J.* 13 (2016) 1309–1314.
- [35] M.A. Najeeb, Z. Ahmad, R.A. Shakoor, Organic thin-film capacitive and resistive humidity sensors: a focus review, *Adv. Mater. Interfaces* 5 (2018) 1800969.
- [36] H. Lee, T.K. Choi, Y.B. Lee, H.R. Cho, R. Ghaffari, L. Wang, H.J. Choi, T.D. Chung, N. Lu, T. Hyeon, S.H. Choi, D.-H. Kim, A graphene-based electrochemical device with thermoresponsive microneedles for diabetes monitoring and therapy, *Nat. Nanotechnol.* 11 (2016) 566–572.
- [37] L.A. Wallace, L. Gwynne, T. Jenkins, Challenges and opportunities of pH in chronic wounds, *Ther. Deliv.* 10 (2019) 719–735.
- [38] Y. Hattori, L. Falgout, W. Lee, S.-Y. Jung, E. Poon, J.W. Lee, I. Na, A. Geisler, D. Sadhwani, Y. Zhang, Y. Su, X. Wang, Z. Liu, J. Xia, H. Cheng, R.C. Webb, A.P. Bonifas, P. Won, J.-W. Jeong, K.-I. Jang, Y.M. Song, B. Nardone, M. Nodzenski, J.A. Fan, Y. Huang, D.P. West, A.S. Paller, M. Alam, W.-H. Yeo, J.A. Rogers, Multifunctional skin-like electronics for quantitative, clinical monitoring of cutaneous wound healing, *Adv. Healthc. Mater.* 3 (2014) 1597–1607.
- [39] Y.-S. Sun, Electrical stimulation for wound-healing: simulation on the effect of electrode configurations, *Biomed. Res. Int.* 2017 (2017) 5289041.
- [40] L. Wang, D. Song, C. Wei, C. Chen, Y. Yang, X. Deng, J. Gu, Telocytes inhibited inflammatory factor expression and enhanced cell migration in LPS-induced skin wound healing models in vitro and in vivo, *J. Transl. Med.* 18 (2020) 60.
- [41] A. Sahu, J. Jeon, M.S. Lee, H.S. Yang, G. Tae, Antioxidant and anti-inflammatory activities of Prussian blue nanozyme promotes full-thickness skin wound healing, *Mater. Sci. Eng. C.* 119 (2021) 111596.
- [42] R. Crompton, H. Williams, D. Ansell, L. Campbell, K. Holden, S. Cruickshank, M.J. Hardman, Oestrogen promotes healing in a bacterial LPS model of delayed cutaneous wound repair, *Lab. Investig.* 96 (2016) 439–449.
- [43] A.M. Rosales, K.S. Anseth, The design of reversible hydrogels to capture extracellular matrix dynamics, *Nat. Rev. Mater.* 1 (2016) 1–15.
- [44] R. Crompton, H. Williams, D. Ansell, L. Campbell, K. Holden, S. Cruickshank, M.J. Hardman, Oestrogen promotes healing in a bacterial LPS model of delayed cutaneous wound repair, *Lab. Investig.* 96 (2016) 439–449.
- [45] L.A. Schneider, A. Korber, S. Grabbe, J. Dissemmond, Influence of pH on wound-healing: a new perspective for wound-therapy? *Arch. Dermatol. Res.* 298 (2007) 413–420.
- [46] D.P. Cuthbertson, W.J. Tilstone, Effect of environmental temperature on the closure of full thickness skin wounds in the rat, *Q. J. Exp. Physiol. Cogn. Med. Sci.* 52 (1967) 249–257.
- [47] M. Rouabhia, H.J. Park, A. Abedin-Do, Y. Douville, M. Méthot, Z. Zhang, Electrical stimulation promotes the proliferation of human keratinocytes, increases the production of keratin 5 and 14, and increases the phosphorylation of ERK1/2 and p38 MAP kinases, *J. Tissue Eng. Regen. Med.* 14 (2020) 909–919.
- [48] J.M. Reinke, H. Sorg, Wound repair and regeneration, *Eur. Surg. Res.* 49 (2012) 35–43.
- [49] S.A. Eming, P. Martin, M. Tomic-Canic, Wound repair and regeneration: mechanisms, signaling, and translation, *Sci. Trans. Med.* 6 (2014) 265sr6.